Replenishment of near-surface water ice by impacts into Ceres' volatile-rich crust: Observations by Dawn's Gamma Ray and Neutron Detector

Thomas H. Prettyman[1], Naoyuki Yamashita[1], Margaret E Landis[2], Julie C Castillo-Rogez[3], Norbert Schorghofer[1], Carle M. Pieters[4], Hanna G. Sizemore[1], Harald Hiesinger[5], Simone Marchi[6], Harry Y McSween[7], Ryan S. Park[3], Michael J Toplis[8], Carol A. Raymond[9], and C. T. Russell[10]

[1]Planetary Science Institute
[2]University of Colorado, Boulder
[3]Jet Propulsion Laboratory
[4]Brown University
[5]Westfälische Wilhelms-Universität Münster
[6]Southwest Research Institute
[7]University of Tennessee at Knoxville
[8]Institut de Recherche en Astrophysique et Planetologie
[9]JPL
[10]University of California, Los Angeles

November 22, 2022

Abstract

Ceres' regolith contains water ice that has receded in response to insolation-driven sublimation. Specially targeted, high spatial-resolution measurements of hydrogen by Dawn's Gamma Ray and Neutron Detector reveal elevated hydrogen concentrations in and around Occator, a young, 90-km diameter, complex crater located at 19.82N where near-surface ice is not expected. The excess hydrogen is explained by impact excavation of water-rich outer crustal materials and their emplacement in the crater floor and ejecta blanket. This is supported by thermophysical models that show water ice could survive at sub-meter depths, given Occator's relatively young age (~20 Myr). We hypothesize that the regolith can be replenished with ice from large impacts and that this process partially controls the distribution and depth of near surface ice. This is supported by results from Occator and similarities in the global distribution of hydrogen and the pattern of large craters (20-100 km diameter).

Replenishment of near-surface water ice by impacts into Ceres' volatile-rich crust: Observations by Dawn's Gamma Ray and Neutron Detector

T. H. Prettyman[1], N. Yamashita[1], M. E. Landis[2], J. C. Castillo-Rogez[3], N. Schörghofer[1], C. M. Pieters[1,4], H. G. Sizemore[1], H. Hiesinger[5], S. Marchi[6], H. Y. McSween[7], R. S. Park,[3] M. J. Toplis[8], C. A. Raymond[3], C. T. Russell[9]

[1]Planetary Science Institute, Tucson, AZ. [2] Laboratory for Atmospheric and Space Physics, University of Colorado, , Boulder, CO. [3]Jet Propulsion Laboratory, California Institute of Technology, Pasadena, CA. [4]Brown University, Providence, RI. [5]Institut für Planetologie, Westfälische Wilhelms-Universität Münster, Münster, Germany. [6]Southwest Research Institute, Boulder, CO. [7]University of Tennessee, Knoxville, TN. [8]L'Institut de Recherche en Astrophysique et Planétologie (University of Toulouse, UT3, CNRS), Toulouse, France. [9]University of California Los Angeles, Los Angeles, CA.

Corresponding author: Thomas Prettyman (prettyman@psi.edu)

Key Points:

- Neutron spectroscopy reveals enhanced hydrogen concentrations in the outermost meter of the surface of a prominent young, complex crater
- Results confirm Ceres outer crust is ice rich and support retention of water ice within impact ejecta on airless, icy bodies
- The data imply partial control of regolith ice content by large impacts, relaxing constraints on surface age and regolith grain size

Abstract

Ceres' regolith contains water ice that has receded in response to insolation-driven sublimation. Specially targeted, high spatial-resolution measurements of hydrogen by Dawn's Gamma Ray and Neutron Detector reveal elevated hydrogen concentrations in and around Occator, a young, 90-km diameter, complex crater located at 19.82N where near-surface ice is not expected. The excess hydrogen is explained by impact excavation of water-rich outer crustal materials and their emplacement in the crater floor and ejecta blanket. This is supported by thermophysical models that show water ice could survive at sub-meter depths, given Occator's relatively young age (~20 Myr). We hypothesize that the regolith can be replenished with ice from large impacts and that this process partially controls the distribution and depth of near surface ice. This is supported by results from Occator and similarities in the global distribution of hydrogen and the pattern of large craters (20-100 km diameter).

Plain Language Summary

The outermost meter of dwarf planet Ceres contains water ice that is gradually sublimating in response to heating of the surface by sunlight. Since Ceres' axis of rotation is nearly perpendicular to the Sun's rays, ice has receded to greater depths at the equator than the poles. The distribution of subsurface ice within this outer layer was inferred from measurements of hydrogen by Dawn's Gamma Ray and Neutron Detector. Special operations during Dawn's last mission phase brought the spacecraft close to the surface, enabling measurements within and around a large, young crater called Occator. Anomalously high concentrations of hydrogen were detected, suggesting the impact that formed Occator excavated water rich materials from the crust and deposited them on the surface. Comparison of the global distribution of hydrogen with the pattern of large craters on Ceres further supports excavation of crustal ice by impacts as a partial control on the depth of ice near the surface. Results confirm that Ceres' crust is rich in water ice and show that ice can survive in materials ejected by impacts into airless, icy bodies.

1 Introduction

The dwarf planet Ceres, the largest body in the main asteroid belt (469.7-km volumetric mean radius), is water rich (Russell et al., 2016). As Ceres evolved, liquid water interacted with rock within the interior to produce hydrated minerals (McSween et al., 2017). Ceres' average interior structure consists of a rocky mantle and a ~40-km thick crust, dominated by the frozen remnants of an ancient, global ocean (Castillo-Rogez et al., 2018; Ermakov et al., 2017). Rheological constraints indicate that the crust is volatile-rich, containing water ice, phyllosilicates, salts, and possibly clathrate hydrates (Fu et al., 2017). Residual brines at the base of the crust could be a source for active cryomagmatism (e.g., Quick et al., 2019; Raymond et al., 2020; Ruesch et al., 2019). High-resolution gravity data imply a positive density gradient in Ceres' crust , interpreted as enrichment of dense oceanic precipitates in the lower part of the crust in contrast to a volatile-rich outer crust (Park et al., 2020).

The ice content of different crustal layers can be inferred from diverse remote-sensing data sets, including nuclear spectroscopy, geomorphology, and gravity. Surficial water ice has been detected within some mid-to-high latitude craters (Combe et al., 2019) and the presence of complex craters with fluidized ejecta, lobate flow features, and pitted terrain indicate water ice is abundant within the few km depths probed by impacts (e.g., Sizemore et al., 2017; 2019).

GRaND measurements reveal the presence of a global ice table within a few millimeters of the surface at the poles that has receded to greater depths at lower latitudes due to increased solar insolation, consistent with Ceres' obliquity history (Prettyman et al., 2017).

Previous analyses of GRaND data support 20 vol.% water ice in the near-surface ice table, with ice below the depth of sensitivity (a few decimeters) near the equator; whereas, the bulk crustal average water content is inferred to be about >60 vol.% based on geophysical measurements of crustal density and strength (Fu et al., 2017; Park et al., 2020). Impact processes are key to understanding the connection between the volatile-rich crustal reservoir and the regolith. A simple-to-complex transition occurs for craters with diameters greater than about 10 km (Hiesinger et al., 2016; Schenk et al., 2021). Furthermore, impacts that formed large craters exposed crustal materials from a wide range of depths within the outer crust, with the excavation depth roughly 10% of the crater diameter (Marchi et al., 2016). As such, large impacts have the potential to redistribute ice within the outer crust.

We use hydrogen mapping data acquired by Dawn's Gamma Ray and Neutron Detector (GRaND) to investigate the effect of impacts on shallow-regolith water ice content. We hypothesize that impacts can bring water ice from the outer crust to the surface, replenishing the regolith with ice. As such, the distribution of near surface water ice in the upper few decimeters of the regolith as sensed by GRaND is shaped both by large impacts and long-term insolation-driven sublimation. We test this hypothesis with high-spatial-resolution GRaND data acquired in Dawn's final mission phase. The high-resolution data are sensitive to the composition of the interior and ejecta blanket of the young, complex crater Occator. Lower-resolution data acquired by GRaND during Dawn's primary mission enable investigations of the global relationships between cratering and regolith hydrogen content.

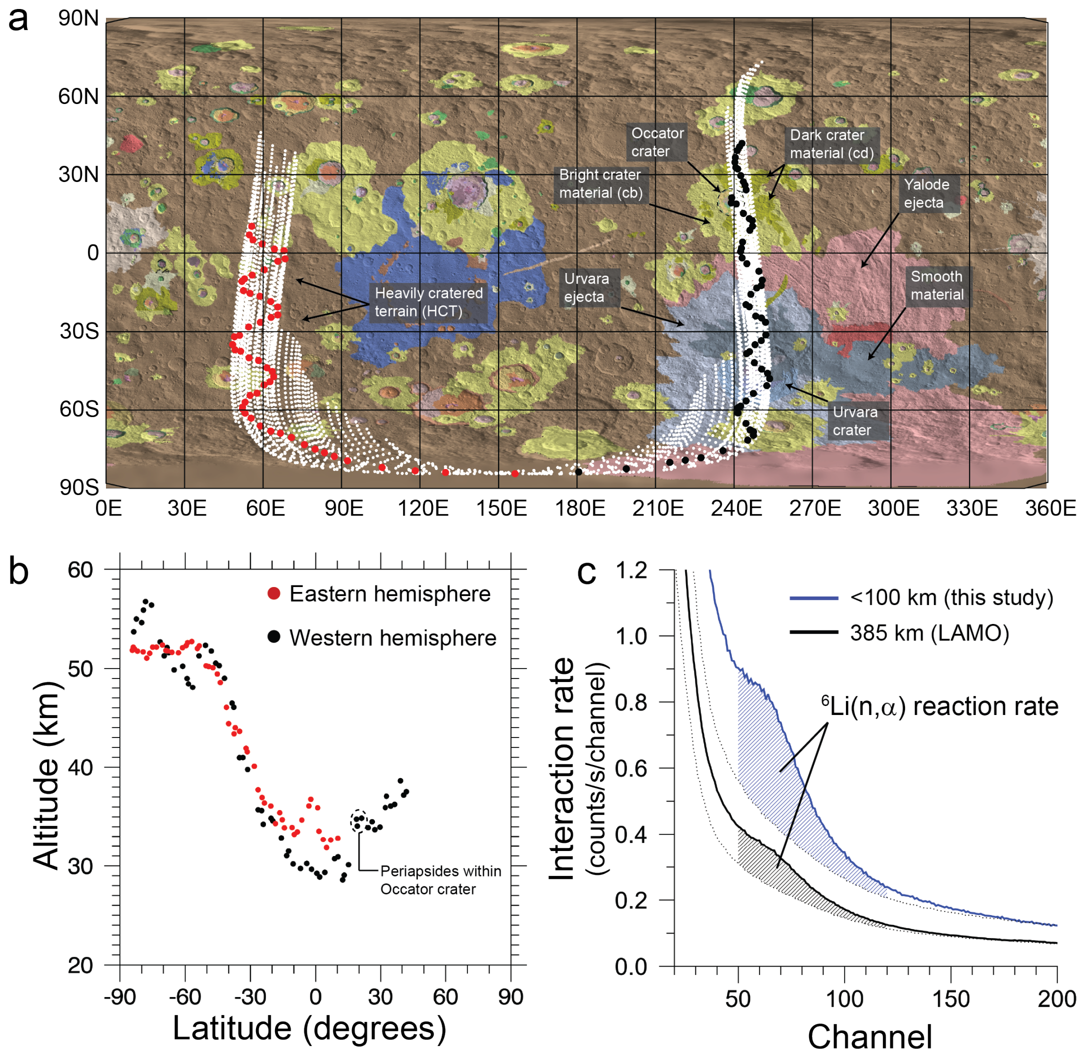

Figure 1. Close-proximity measurements. **(a)** Highly eccentric orbits (south-north trajectory) enabled the acquisition of GRaND data with 35s accumulation intervals at over 5000 locations with altitudes less than 100 km (white points). Circles (red and black) indicate the measurement locations closest to the periapsides of the 113 orbits used in the analysis (Text S1). The measurements sampled geologic units in the eastern and western hemispheres along the 60E and 240E meridian, including the ~20 Myr old Occator crater (Neesemann et al., 2019), centered at 239.33E and 19.82N, and its ejecta blanket. See Williams et al. (2019) for geological unit definitions. (**b**) Altitudes of periapsis less than 30 km were achieved at some locations near the equator, with higher altitudes towards the poles. **(c)** Close proximity enabled acquisition of neutron counting data with high spatial resolution and precision. The ^{6}Li(n,α) reaction rate in GRaND's lithium-loaded glass (LiG) scintillator (shaded areas) is sensitive to regolith hydrogen content (Text S1). The average reaction rate below 100 km was about 3× higher than observed in Dawn's low altitude mapping orbit (LAMO).

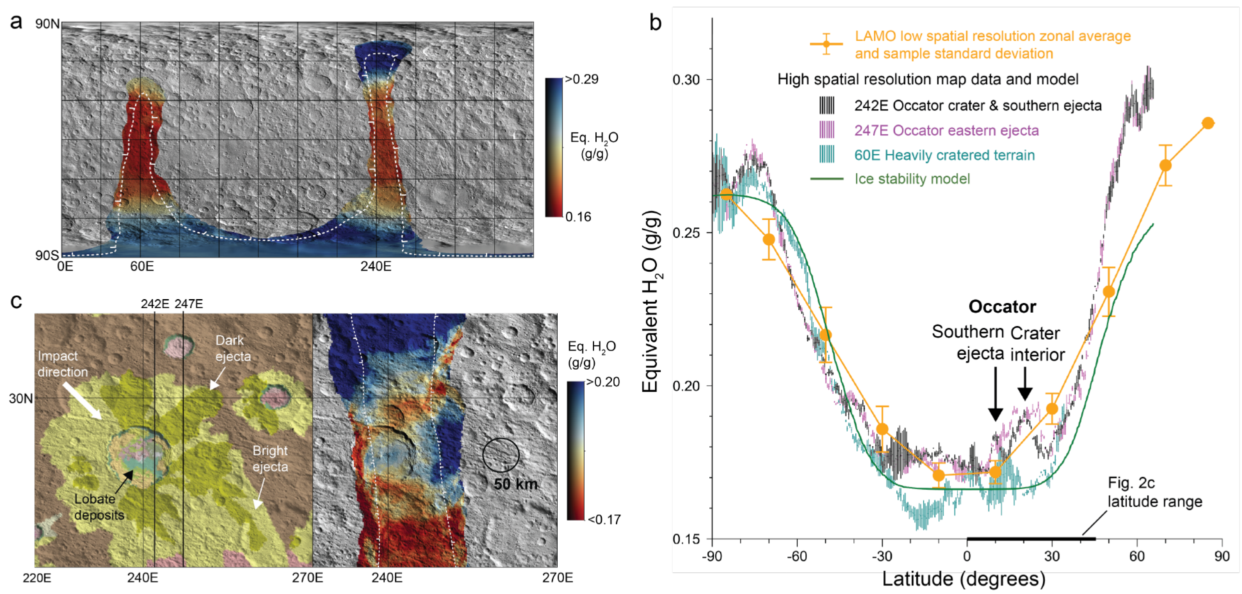

Figure 2. Distribution of subsurface hydrogen. **(a)** The equirectangular map of water-equivalent hydrogen, was determined from ^{6}Li(n,α) reaction rates measured below 100 km altitude. The white contour line, which approximates the boundary of the point cloud in Fig. 1a, delineates the most highly sampled region, with contributions from >50 measurements at each map location. Outside the point cloud, hydrogen concentrations are extrapolated from the data. (**b)** The distribution of hydrogen in **(a)** is plotted for selected meridians. The population standard deviation in hydrogen concentration, determined by Monte Carlo error propagation, is represented by vertical lines. The distribution of hydrogen, which is more variable than the LAMO zonal average (Prettyman et al., 2017) is consistent with a globally receding ice table. The mapping algorithm was applied to simulated, low-altitude neutron measurements of the distribution of ice determined by thermophysical modeling (i.e., ice-cemented soil with 1 μm grain size, 0.2 porosity, and 10 wt.% water ice) (Prettyman et al., 2017). These parameters produced a close match to the neutron counting data acquired in LAMO. (**c)** The low-altitude data reveal elevated concentrations of hydrogen in and around Occator crater. Map variations on spatial scales greater than 50 km (black circle) can be interpreted as changes in subsurface composition. A geologic map of the Occator region is provided for context (Scully et al., 2019; Williams et al., 2018, with units defined therein). Map data are superimposed on shaded relief.

2 Hydrogen mapping with high spatial resolution GRaND data

In Dawn's final mission phase, the spacecraft maneuvered into a highly eccentric orbit with low periapsis (30-50 km, Figs. 1a, 1b and Text S1). This enabled acquisition of high-spatial-resolution GRaND data, on scales comparable to geologic units over a wide range of latitudes in both the eastern and western hemispheres. Analyses of high resolution data can be compared with the elemental measurements determined from GRaND data acquired in Dawn's primary mission from a low altitude mapping orbit (LAMO) with 385 km mean altitude

(Prettyman et al., 2017). Since spatial resolution scales with altitude (Prettyman et al., 2019), the eccentric orbits achieved up to 10× improvement in spatial resolution compared to LAMO.

A primary target of the eccentric orbits was Occator crater, a very young (<20 Myr) (Neesemann et al., 2019) 90-km diameter, complex crater located at about 19.82N and 239.33E within Hanami Planum. The crater contains prominent faculae as well as lobate deposits and fluidized ejecta, which likely contain water ice (Scully et al., 2019). Thus, the geomorphology supports impact into an ice-rich substrate. The crater and immediate surroundings were well sampled with multiple orbits with periapsides near 35-km altitude, corresponding to an intrinsic spatial resolution of about 50 km full-width-at-half-maximum for GRaND. This allowed measurements of hydrogen within the crater interior and portions of the ejecta blanket, providing constraints on processes underlying crater formation and the fate of hydrogen-bearing materials.

The concentration of hydrogen was determined from the leakage flux of low-energy neutrons produced by the interaction of galactic cosmic rays (GCRs) with Ceres' regolith. Measurements of the ^{6}Li(n,α) reaction rate with GRaND's +Z lithium-loaded glass (LiG) scintillator (Prettyman et al., 2011) provide a high intensity signal from which the concentration of hydrogen can be determined with high precision and accuracy (Fig. 1c) (Prettyman et al., 2017). This signal was used to map hydrogen on fine spatial scales using data acquired below 100-km altitude.

Text S1 and S2 describe the data reduction and mapping methods. The ^{6}Li(n,α) reaction rate at each orbital location was determined and corrected for variations in the flux of GCRs using data acquired near the apoapsis of each orbit. Corrections for measurement geometry were made using the forward model described by Prettyman et al. (2017) that accounts for Ceres' overall shape and local topography when the spacecraft was in close proximity to the surface. The corrected counting data were mapped onto the surface using a circle superposition algorithm that accounts for variations in the resolution of the spectrometer with altitude. High-resolution maps are shown in Fig. 2.

To validate the sensitivity of the elliptical data to the interior of Occator crater, we averaged the ^{6}Li(n,α) counts for three nearly identical orbits with periapsides near the center of the crater (Fig. S1). The data reveal a significant suppression of counts within the crater and to the south of the crater, consistent with mapped enhancements in hydrogen shown in Fig. 2b.

Furthermore, simulations of the response of GRaND to neutrons emitted within geologic units (Fig. S1) supports the sensitivity of the measurements to ice in the lobate deposits and terrace material inside the crater as well as ice in the ejecta blanket.

3 Results

The high spatial resolution maps reveal similar large-scale trends as observed in LAMO (Prettyman et al., 2017) with more hydrogen at high latitudes than near the equator (Figs. 2a, 2b and 3c). This pattern is consistent with the presence of a receding ice table. If the regolith initially contained ice-cemented soil, then the LAMO data can be explained by a low-diffusivity regolith with about 0.2 porosity and 1 μm grain size (Prettyman et al., 2017). In this case, ice is expected to have receded to about 80-90 cm at the equator over Ceres' lifetime. Ice would have been preserved at submillimeter depths poleward of 60 degrees latitude in the northern and southern hemispheres.

Forward modeling was used to determine the concentration of hydrogen that would have been observed by GRaND from the eccentric orbit given the distribution of ice that best fits the LAMO data per Prettyman et al. (2017) (green curve in Fig. 2b). The modeled variation in bulk regolith hydrogen approximates the observed variation in the high-resolution data at southern high latitudes. Near the equator (±30 degrees latitude), the model is nearly constant, indicating ice in this region at depths greater than sensed by GRaND. Within this region, the "best fit" model ice depths from Prettyman et al. (2017) ranged from 50-90 centimeters.

In contrast to the model, the high-resolution measurements show variations in hydrogen content with latitude and longitude in the equatorial band. For example, the concentration of hydrogen at low latitudes in eastern and western hemispheres differs by up to 4 wt.% (Fig. 2b). Lower concentrations of hydrogen in the eastern hemisphere are consistent with LAMO observations (Prettyman et al., 2017); however, the high-resolution data reveal small scale variability, including enhanced concentrations of hydrogen in the Occator region (up to 2 wt.% eq. H_2O higher than surroundings). The northern hemisphere has more hydrogen than in the south and hydrogen at high latitudes increases more steeply in the north, perhaps indicating a larger gradient in ice table depth or ice concentration with latitude. The vertical lines that represent the statistical uncertainty in the data (Fig. 2b) indicate these variations are significant.

A map of the distribution of hydrogen in the Occator region (Fig. 2c) shows that Occator's interior and portions of the ejecta blanket to the east and south of the crater are richer in hydrogen than the surrounding low latitude region. Geologic mapping shows that Occator's ejecta blanket is asymmetrical, suggesting an oblique impact from the northwest (Scully et al., 2019). Relatively hydrogen-poor materials extend from the northern rim of the crater to the northeast, which partially overlaps a lane of dark ejecta shown in the geologic map (Fig. 2c). Otherwise, the observed distribution of hydrogen is not closely aligned with geologic units.

4 Discussion

Hydrogen within Ceres' regolith is in the form of hydrated minerals, water ice, and other hydrogen-bearing species. Spectral mixing fractions were determined for a suite of detected minerals (Raponi et al., 2019). These included Mg-, Al-, and NH_4-bearing phyllosilicates, Mg- and Na-carbonates, NH_4-chloride, and a darkening agent. Following Marchi et al. (2019), the spectral mixing fractions were interpreted as volume fractions and combined with mineral densities and empirical formulae to estimate the concentration of hydrogen at Occator (Text S3). Both VIR and GRaND maps show a lobe of hydrogen-poor material extending to the northeast from the northern rim of the crater (Fig. 3). Otherwise, they have dissimilar distributions and ranges, most likely due to differences in the hydration state of the regolith layers sensed by the instruments. VIR is sensitive to the uppermost ~100 μm surface layer; whereas, GRaND is sensitive to the uppermost meter. The presence of subsurface ice could account for the comparatively high dynamic range of GRaND data.

Outside the faculae, the VIR-derived hydrogen concentration spans 16-17 wt.% eq. H_2O, similar to the lowest values reported by GRaND (Fig. 3a). Natrite (Na_2CO_3) is a significant component of the faculae (Raponi et al., 2019). It was suggested that Na-carbonates were initially hydrated (e.g., Zolotov, 2017); however, these hydrated species are not stable within the shallow subsurface within Occator crater (Text S4). As such, the faculae must be hydrogen poor (estimated to be <10 wt.% eq. H_2O, ignoring bound water) compared to dark background materials. The faculae cover a small portion of the crater floor, well below the spatial scales resolved by GRaND even at closest approach (Fig. S1). Consequently, within the crater hydrated salts are not likely a significant contributor to the hydrogen measured by GRaND.

Global variations in regolith hydrogen content, including the observed N-S and E-W differences (Fig. 2), are not likely the result of variations in the concentration of hydrated minerals. The dynamic range of VIR 2.7- and 3.1-μm band depths (OH and NH_4, respectively) is about one fifth that of subsurface hydrogen on the broad spatial scales sampled by GRaND in LAMO (Ammannito et al., 2016; Prettyman et al., 2019). Some variability in subsurface hydrogen may result from the presence of water bound to salts or interlayer water in clay minerals. Nevertheless, detections of hydrated sodium carbonate are rare (Tosi et al., 2018) and if present may be in a low hydration state as nahcolite (Zolotov, 2017). Hydrated chloride salts, which could represent a significant crustal component depending on the freezing state of the ocean are not likely to be abundant in the shallow subsurface and regolith (Castillo-Rogez et al., 2018). Hydrohalite reported at Cerealia Tholus by De Sanctis et al. (2020) is hypothesized to originate from the deep brine reservoir source of the Occator faculae (Raymond et al., 2020).

Relatively high concentrations of hydrogen in the interior of Occator crater and its ejecta blanket likely result from the presence of subsurface water ice. Lobate deposits cover a significant portion (>30%) of the crater floor (Fig. 2c) and may contain high concentrations of water ice (Scully et al., 2019). These likely formed following the impact by mixing of crustal water with rock to produce a water-rich slurry that filled portions of the crater's floor (Raponi et al., 2019; Scully et al., 2019). A portion of the excavated water would have been emplaced in the ejecta blanket (Schröder et al., 2021). The heterogeneous distribution of hydrogen enhancements in and around Occator likely represents variations in the composition of materials ejected by the impact and their thermal history.

Thermophysical modeling shows that buried water ice, if present following impact, could still be found at depths sensed by GRaND in both the lobate deposits and the ejecta blanket, given Occator's ~20 Myr age (Neesemann et al., 2019) and a plausible range of regolith physical properties (Fig. 3b). Grain sizes determined by VIR in the Occator region are greater than 30 μm (Raponi et al., 2019), which would result in much higher vapor diffusivity than inferred from GRaND data acquired in LAMO (Prettyman et al., 2017). Consequently, the coarse grain sizes modeled in Fig. 3b provide an upper limit on the expected ice depths.

The global N-S asymmetry in hydrogen on Ceres suggests hemispheric differences in regolith ice content. This asymmetry cannot be explained by a receding ice table given Ceres' precessing orbital elements and reasonable models of surface roughness (Hayne & Aharonson, 2015; Landis et al., 2017; Prettyman et al., 2017; Schorghofer, 2016). Nevertheless, the detection of elevated hydrogen concentrations within and around Occator provides evidence for water ice emplaced in the regolith during the formation of large craters. We assess whether this process could influence the global distribution of hydrogen.

Hiesinger et al. (2016) catalogued craters greater than 20-diameter. Craters in the 20-100-km range sample the outer ~2- to 10-km of the crust, a layer potentially rich in water ice (Park et al., 2020). The density of these craters when smoothed to the spatial resolution of GRaND exhibits a N-S asymmetry, like hydrogen, with highest density in the northern hemisphere (Fig. 4a). In addition, elevated hydrogen concentrations extending from the northern to the southern hemisphere roughly corresponds with craters centered at 180E (Fig. S2). These associations suggest that the global distribution of hydrogen could be controlled – at least in part – by excavation of ice by large impacts; however, this hypothesis cannot fully explain the observed variability in hydrogen concentration (Fig. S3). Impact basins excluded from the crater density map, would have excavated deeper crustal materials perhaps with lower water content, modifying the composition of the regolith and crust in large portions of the eastern and southern hemisphere (e.g., Lawrence et al., 2018). Hidden basins (> 280 km in diameter) would have dominated early regolith production and could also contribute to large-scale variations in the distribution of hydrogen (Marchi et al., 2016).

Previous work considered insolation-driven retreat of ice over the 4.5 Gyr lifetime of Ceres (Prettyman et al., 2017). Models predict that modification of the ice table depth by impact gardening is negligible (Costello et al., 2021; Schorghofer, 2016). As such, the GRaND hydrogen data support relatively shallow ice depths (~90 centimeters at the equator), with low inferred regolith vapor diffusivity (effective grain size of 1 μm and 0.2 porosity, Fig. 4b). The presence of μm-size particles is supported by spectrophotometry (Li et al., 2019). This contrasts with 10-100 μm grains derived from infrared observations (Gundlach & Blum, 2013; Raponi et al., 2019). For fixed porosity, vapor diffusivity increases with grain size (Schorghofer, 2016). The ice depths inferred by GRaND can be explained if larger grain sizes are present, but only if the ice was emplaced more recently than 4.5 Gyr. For example, ice deposited ~500 Myr ago would have retreated to 90 centimeters depth at the equator if the grain size were 10 μm.

Consequently, delivery of crustal ice to the regolith by impacts could influence the depth of near-surface ice. Assuming granular segregation with depth within the regolith can be ignored, this could allow reconciliation of GRaND and VIR inferences of grain size.

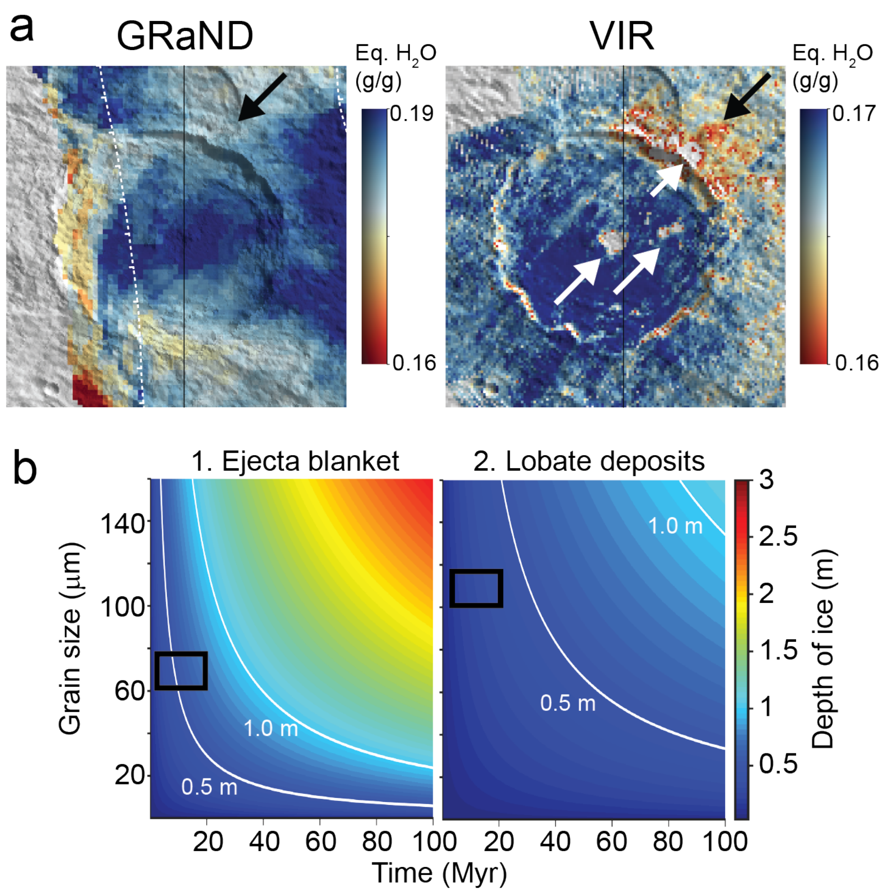

Figure 3. Evidence for water ice at Occator crater. **(a)** The distribution of hydrogen within and immediately surrounding Occator determined by GRaND is compared to that inferred from VIR mineralogy (Text S3) (Marchi et al., 2019; Raponi et al., 2019). The VIR-derived hydrogen concentration within the facula and portions of the crater rim is <16 wt.% eq. H_2O (white arrows point to regions with no data in the range indicated by the scalebar). The faculae are smaller than can be resolved by GRaND. Both maps include a lobe of relatively hydrogen-poor material extending from the north and east of the crater (black arrows). **(b)** Thermophysical modeling shows that ice could survive at depths sensed by GRaND for a range of reported ages (Neesemann et al., 2019) and feasible regolith thermophysical properties (porosity and grain size) . Two cases are modeled: 1. Impact ejecta emplaced outside the crater are assumed to have the same porosity (0.2) as determined by GRaND in LAMO. 2. Within the interior of the crater, ice may have been concentrated in lobate deposits during crater formation (Scully et al., 2019) (90% water by volume, with an overlying sublimation lag with a porosity of 0.5). Boxes indicate the most likely range of ages and VIR-derived grain sizes (Raponi et al., 2019).

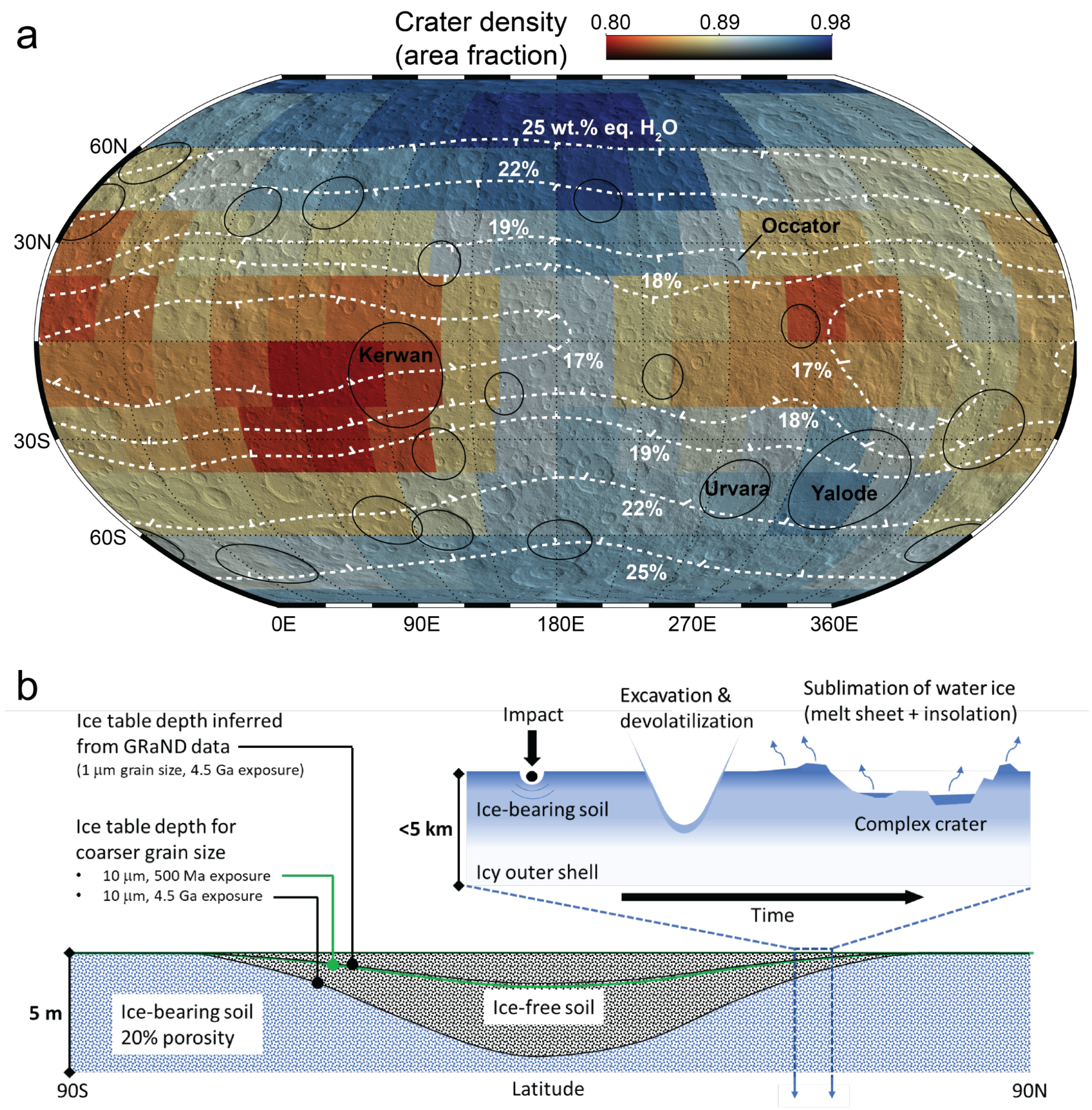

Figure 4. Impact processes as a partial control on the global distribution of hydrogen. **(a)** A map of the density of large craters is compared to the global distribution of hydrogen measured by GRaND (white contours). The map was determined by smoothing the pattern of large craters (20- to 100-km diameter) catalogued by Hiesinger et al. (2016) to the spatial resolution of GRaND in LAMO using the smoothing algorithm of Prettyman et al. (2019). A density of 1 indicates craters fully cover the surface within GRaND's field of view. For context, the map is superimposed on shaded relief and excluded basins with diameters greater than 100 km are outlined (black). Associations between crater density and the global distribution of hydrogen are detailed in Figs. S2 and S3. **(b)** A possible scenario for enrichment of surficial ice by large impacts is illustrated. A portion of the ice excavated from the crust survives during crater formation and cooling of the melt sheet and ejecta blanket, enriching the regolith in water ice. The surviving ice retreats in response to solar insolation.

5 Conclusions

Our analysis suggests the distribution of water ice within Ceres' bulk regolith is controlled by a combination of insolation-driven sublimation and delivery of water-bearing materials to the regolith from the volatile-rich outer crust by large impacts. The observed enrichment in hydrogen within Occator cater and ejecta blanket shows that excavated ice not only survives large impacts but also enhances the concentration of ice in the shallow subsurface. Associations between the pattern of large craters and the distribution of hydrogen suggest this process could be pervasive on Ceres. Impact replenishment of the regolith with crustal ice would allow the GRaND data to be explained by younger surface ages with larger regolith grain sizes more consistent with those inferred from infrared spectroscopy.

The high-resolution GRaND data support an endogenic crustal origin for ice within the regolith. Since the excavation depth of Occator was nearly 10 km , our results bring direct evidence for a large amount of ice in Ceres' crust, consistent with indirect inferences from geological observations (e.g., Sizemore et al., 2019). Alternative interpretations of the Dawn geophysical data in terms of an ice-free Ceres (Zolotov, 2020) are thus inconsistent with the GRaND data. The results also support the recent interpretation proposed by Schröder et al. (2021) for the distinctly blue color of ejecta from recent impact craters as an evolved mixture of ice and minerals.

Acknowledgments

Funding was provided by the NASA Discovery Data Analysis Program, the NASA SSERVI Toolkit for Research and Exploration project, and the NASA Dawn Mission. Part of this work was carried out at the Jet Propulsion Laboratory, California Institute of Technology, under contract to NASA. We thank B. L. Ehlmann for contributions to the interpretation of the data. The Dawn Flight Team acquired the special, high-resolution data set used in this study. The GRaND data are available from the NASA Planetary Data System at https://sbn.psi.edu/pds/resource/dawn/dawngrandPDS4.html.

References

Ammannito, E., DeSanctis, M. C., Ciarniello, M., Frigeri, A., Carrozzo, F. G., Combe, J.-P., et al. (2016). Distribution of phyllosilicates on the surface of Ceres. *Science, 353*(6303), aaf4279. doi:10.1126/science.aaf4279

Bu, C., Rodriguez Lopez, G., Dukes, C. A., McFadden, L. A., Li, J. Y., & Ruesch, O. (2018a). Stability of hydrated carbonates on Ceres. *Icarus, 320*, 136-149. doi:https://doi.org/10.1016/j.icarus.2017.12.036

Bu, C., Rodriguez Lopez, G., Dukes, C. A., Ruesch, O., McFadden, L. A., & Li, J. Y. (2018b). Search for sulfates on the surface of Ceres. *Meteoritics & Planetary Science, 53*(9), 1946-1960. doi:10.1111/maps.13024

Carrozzo, F. G., De Sanctis, M. C., Raponi, A., Ammannito, E., Castillo-Rogez, J., Ehlmann, B. L., et al. (2018). Nature, formation, and distribution of carbonates on Ceres. *Science Advances, 4*(3), e1701645. doi:10.1126/sciadv.1701645

Castillo-Rogez, J., Neveu, M., McSween, H. Y., Fu, R. R., Toplis, M. J., & Prettyman, T. (2018). Insights into Ceres's evolution from surface composition. *Meteoritics & Planetary Science, 53*(9), 1820-1843. doi:10.1111/maps.13181

Combe, J.-P., Raponi, A., Tosi, F., De Sanctis, M. C., Carrozzo, F. G., Zambon, F., et al. (2019). Exposed H2O-rich areas detected on Ceres with the dawn visible and infrared mapping spectrometer. *Icarus, 318*, 22-41. doi:10.1016/j.icarus.2017.12.008

Costello, E. S., Ghent, R. R., & Lucey, P. G. (2021). Impact Gardening on Ceres. *Geophysical Research Letters, n/a*(n/a), e2021GL092960. https://doi.org/10.1029/2021GL092960. doi:https://doi.org/10.1029/2021GL092960

De Sanctis, M. C., Ammannito, E., Raponi, A., Marchi, S., McCord, T. B., McSween, H. Y., et al. (2015). Ammoniated phyllosilicates with a likely outer Solar System origin on (1) Ceres. *Nature, 528*(7581), 241-244. doi:10.1038/nature16172

De Sanctis, M. C., Ammannito, E., Raponi, A., Frigeri, A., Ferrari, M., Carrozzo, F. G., et al. (2020). Fresh emplacement of hydrated sodium chloride on Ceres from ascending salty fluids. *Nature Astronomy, 4*(8), 786-793. doi:10.1038/s41550-020-1138-8

Ermakov, A. I., Fu, R. R., Castillo-Rogez, J. C., Raymond, C. A., Park, R. S., Preusker, F., et al. (2017). Constraints on Ceres' internal structure and evolution from its shape and gravity measured by the Dawn spacecraft. *Journal of Geophysical Research: Planets, 122*(11), 2267-2293. doi:10.1002/2017je005302

Fu, R. R., Ermakov, A. I., Marchi, S., Castillo-Rogez, J. C., Raymond, C. A., Hager, B. H., et al. (2017). The interior structure of Ceres as revealed by surface topography. *Earth and Planetary Science Letters, 476*, 153-164. doi:10.1016/j.epsl.2017.07.053

Gundlach, B., & Blum, J. (2013). A new method to determine the grain size of planetary regolith. *Icarus, 223*(1), 479-492. doi:https://doi.org/10.1016/j.icarus.2012.11.039

Haines, E. L., Etchegaray-Ramirez, M. I., & Metzger, A. E. (1978). Thorium concentrations in the lunar surface. II: Deconvolution modeling and its application to the regions of Aristarchus and Mare Smythii. *Proc. Lunar Planet. Sci. Conf. 9th*, 2985-3013.

Hayne, P. O., & Aharonson, O. (2015). Thermal stability of ice on Ceres with rough topography. *Journal of Geophysical Research: Planets, 120*(9), 1567-1584. doi:10.1002/2015je004887

Hiesinger, H., Marchi, S., Schmedemann, N., Schenk, P., Pasckert, J. H., Neesemann, A., et al. (2016). Cratering on Ceres: Implications for its crust and evolution. *Science, 353*(6303), aaf4759. doi:10.1126/science.aaf4759

Landis, M. E., Byrne, S., Schörghofer, N., Schmidt, B. E., Hayne, P. O., Castillo-Rogez, J., et al. (2017). Conditions for sublimating water ice to supply Ceres' exosphere. *Journal of Geophysical Research: Planets, 122*(10), 1984-1995. doi:10.1002/2017JE005335

Landis, M. E., Byrne, S., Combe, J.-P., Marchi, S., Castillo-Rogez, J., Sizemore, H. G., et al. (2019). Water vapor contribution to Ceres' exosphere from observed surface ice and postulated ice-exposing impacts. *Journal of Geophysical Research: Planets, 124*(1), 61-75. doi:10.1029/2018je005780

Lawrence, D., Elphic, R., Feldman, W., Prettyman, T., Gasnault, O., & Maurice, S. (2003). Small-area thorium features on the lunar surface. *Journal of Geophysical Research, 108*(E9), 5102.

Lawrence, D. J., Peplowski, P. N., Beck, A. W., Feldman, W. C., Prettyman, T. H., Russell, C. T., et al. (2018). Compositional variability on the surface of 1 Ceres revealed through GRaND measurements of high-energy gamma rays. *53*(9), 1805-1819. doi:doi:10.1111/maps.13124

Li, J.-Y., Reddy, V., Nathues, A., Corre, L. L., Izawa, M. R. M., Cloutis, E. A., et al. (2016). Surface albedo and spectral variability of Ceres. *The Astrophysical Journal, 817*(2), L22. doi:10.3847/2041-8205/817/2/l22

Li, J.-Y., Schröder, S. E., Mottola, S., Nathues, A., Castillo-Rogez, J. C., Schorghofer, N., et al. (2019). Spectrophotometric modeling and mapping of Ceres. *Icarus, 322*, 144-167. doi:https://doi.org/10.1016/j.icarus.2018.12.038

Marchi, S., Ermakov, A. I., Raymond, C. A., Fu, R. R., O'Brien, D. P., Bland, M. T., et al. (2016). The missing large impact craters on Ceres. *Nature Communications, 7*, 12257. Article. doi:10.1038/ncomms12257

Marchi, S., Raponi, A., Prettyman, T. H., De Sanctis, M. C., Castillo-Rogez, J., Raymond, C. A., et al. (2019). An aqueously altered carbon-rich Ceres. *Nature Astronomy, 3*(2), 140-145. doi:10.1038/s41550-018-0656-0

Maurice, S., Lawrence, D. J., Feldman, W. C., Elphic, R. C., & Gasnault, O. (2004). Reduction of neutron data from Lunar Prospector. *Journal of Geophysical Research: Planets, 109*(E7). doi:doi:10.1029/2003JE002208

McCord, T. B., Orlando, T. M., Teeter, G., Hansen, G. B., Sieger, M. T., Petrik, N. G., & Van Keulen, L. (2001). Thermal and radiation stability of the hydrated salt minerals epsomite, mirabilite, and natron under Europa environmental conditions. *Journal of Geophysical Research, 106*(E2), 3311-3319. doi:doi:10.1029/2000JE001282

McKinney, G. W., Lawrence, D. J., Prettyman, T. H., Elphic, R. C., Feldman, W. C., & Hagerty, J. J. (2006). MCNPX benchmark for cosmic ray interactions with the Moon. *Journal of Geophysical Research, 111*(E6), E06004. doi:10.1029/2005je002551

McSween, H. Y., Emery, J. P., Rivkin, A. S., Toplis, M. J., C. Castillo-Rogez, J., Prettyman, T. H., et al. (2017). Carbonaceous chondrites as analogs for the composition and alteration of Ceres. *Meteoritics & Planetary Science, 53*(8), 1793-1804. doi:10.1111/maps.12947

Neesemann, A., van Gasselt, S., Schmedemann, N., Marchi, S., Walter, S. H. G., Preusker, F., et al. (2019). The various ages of Occator crater, Ceres: Results of a comprehensive synthesis approach. *Icarus, 320*, 60-82. doi:10.1016/j.icarus.2018.09.006

Park, R. S., & Buccino, D. R. (2018). Ceres SPC Shape Model Dataset V1.0, DAWN-A-FC2-5-CERESSHAPESPC-V1.0. *NASA Planetary Data System*.

Park, R. S., Vaughan, A. T., Konopliv, A. S., Ermakov, A. I., Mastrodemos, N., Castillo-Rogez, J. C., et al. (2019). High-resolution shape model of Ceres from stereophotoclinometry using Dawn Imaging Data. *Icarus, 319*, 812-827. doi:10.1016/j.icarus.2018.10.024

Park, R. S., Konopliv, A. S., Ermakov, A. I., Castillo-Rogez, J. C., Fu, R. R., Hughson, K. H. G., et al. (2020). Evidence of non-uniform crust of Ceres from Dawn's high-resolution gravity data. *Nature Astronomy, 4*(8), 748-755. doi:10.1038/s41550-020-1019-1

Prettyman, T. H., Feldman, W. C., & Titus, T. N. (2009). Characterization of Mars' seasonal caps using neutron spectroscopy. *Journal of Geophysical Research, 114*(E8). doi:10.1029/2008je003275

Prettyman, T. H., Feldman, W. C., McSween, H. Y., Jr., Dingler, R. D., Enemark, D. C., Patrick, D. E., et al. (2011). Dawn's gamma ray and neutron detector. *Space Science Reviews, 163*(1), 371-459. doi:10.1007/s11214-011-9862-0

Prettyman, T. H., Mittlefehldt, D. W., Yamashita, N., Lawrence, D. J., Beck, A. W., Feldman, W. C., et al. (2012). Elemental mapping by Dawn reveals exogenic H in Vesta's regolith. *Science, 338*(6104), 242-246. doi:10.1126/science.1225354

Prettyman, T. H., Yamashita, N., Toplis, M. J., McSween, H. Y., Schorghofer, N., Marchi, S., et al. (2017). Extensive water ice within Ceres' aqueously altered regolith: Evidence from nuclear spectroscopy. *Science, 355*(6320), 55-59. doi:10.1126/science.aah6765

Prettyman, T. H., Yamashita, N., Ammannito, E., Ehlmann, B. L., McSween, H. Y., Mittlefehldt, D. W., et al. (2019). Elemental composition and mineralogy of Vesta and Ceres: Distribution and origins of hydrogen-bearing species. *Icarus, 318*, 42-55. doi:10.1016/j.icarus.2018.04.032

Quick, L. C., Buczkowski, D. L., Ruesch, O., Scully, J. E. C., Castillo-Rogez, J., Raymond, C. A., et al. (2019). A possible brine reservoir beneath Occator Crater: Thermal and compositional evolution and formation of the Cerealia dome and Vinalia Faculae. *Icarus, 320*, 119-135. doi:10.1016/j.icarus.2018.07.016

Raponi, A., De Sanctis, M. C., Carrozzo, F. G., Ciarniello, M., Castillo-Rogez, J. C., Ammannito, E., et al. (2019). Mineralogy of Occator crater on Ceres and insight into its evolution from the properties of carbonates, phyllosilicates, and chlorides. *Icarus, 320*, 83-96. doi:10.1016/j.icarus.2018.02.001

Raymond, C. A., Ermakov, A. I., Castillo-Rogez, J. C., Marchi, S., Johnson, B. C., Hesse, M. A., et al. (2020). Impact-driven mobilization of deep crustal brines on dwarf planet Ceres. *Nature Astronomy, 4*(8), 741-747. doi:10.1038/s41550-020-1168-2

Rivkin, A. S., Li, J.-Y., Milliken, R. E., Lim, L. F., Lovell, A. J., Schmidt, B. E., et al. (2011). The Surface Composition of Ceres. In C. Russell & C. Raymond (Eds.), *The Dawn Mission to Minor Planets 4 Vesta and 1 Ceres* (pp. 95-116). New York, NY: Springer New York.

Ruesch, O., Genova, A., Neumann, W., Quick, L. C., Castillo-Rogez, J. C., Raymond, C. A., et al. (2019). Slurry extrusion on Ceres from a convective mud-bearing mantle. *Nature Geoscience, 12*(7), 505-509. doi:10.1038/s41561-019-0378-7

Russell, C. T., Raymond, C. A., Ammannito, E., Buczkowski, D. L., De Sanctis, M. C., Hiesinger, H., et al. (2016). Dawn arrives at Ceres: Exploration of a small, volatile-rich world. *Science, 353*(6303), 1008-1010. doi:10.1126/science.aaf4219

Schenk, P., Castillo-Rogez, J., Otto, K. A., Marchi, S., O'Brien, D., Bland, M., et al. (2021). Compositional control on impact crater formation on mid-sized planetary bodies: Dawn at Ceres and Vesta, Cassini at Saturn. *Icarus, 359*, 114343. doi:https://doi.org/10.1016/j.icarus.2021.114343

Schorghofer, N. (2008). The lifetime of ice on main belt asteroids. *Astrophysical Journal, 682*(1), 697-705. doi:10.1086/588633

Schorghofer, N. (2016). Predictions of depth-to-ice on asteroids based on an asynchronous model of temperature, impact stirring, and ice loss. *Icarus, 276*, 88-95. doi:10.1016/j.icarus.2016.04.037

Schröder, S. E., Poch, O., Ferrari, M., Angelis, S. D., Sultana, R., Potin, S. M., et al. (2021). Dwarf planet (1) Ceres surface bluing due to high porosity resulting from sublimation. *Nature Communications, 12*(1), 274. doi:10.1038/s41467-020-20494-5

Scully, J. E. C., Buczkowski, D. L., Raymond, C. A., Bowling, T., Williams, D. A., Neesemann, A., et al. (2019). Ceres' Occator crater and its faculae explored through geologic mapping. *Icarus, 320*, 7-23. doi:10.1016/j.icarus.2018.04.014

Sizemore, H. G., Platz, T., Schorghofer, N., Prettyman, T. H., De Sanctis, M. C., Crown, D. A., et al. (2017). Pitted terrains on (1) Ceres and implications for shallow subsurface volatile distribution. *Geophys Res Lett, 44*(13), 6570-6578. doi:10.1002/2017GL073970

Sizemore, H. G., Schmidt, B. E., Buczkowski, D. A., Sori, M. M., Castillo-Rogez, J. C., Berman, D. C., et al. (2019). A Global Inventory of Ice-Related Morphological Features on Dwarf Planet Ceres: Implications for the evolution and current state of the cryosphere. *Journal of Geophysical Research: Planets*. doi:10.1029/2018JE005699

Tosi, F., Carrozzo, F. G., Raponi, A., De Sanctis, M. C., Thangjam, G., Zambon, F., et al. (2018). Mineralogy and temperature of crater Haulani on Ceres. *Meteoritics & Planetary Science, 53*(9), 1902-1924. https://doi.org/10.1111/maps.13078. doi:https://doi.org/10.1111/maps.13078

Williams, D. A., Buczkowski, D. L., Mest, S. C., Scully, J. E. C., Platz, T., & Kneissl, T. (2018). Introduction: The geologic mapping of Ceres. *Icarus, 316*, 1-13. doi:https://doi.org/10.1016/j.icarus.2017.05.004

Williams, D. A., Buczkowski, D. L., Crown, D. A., Frigeri, A., Hughson, K., Kneissl, T., et al. (2019). Final Dawn LAMO-based global geologic map of Ceres. *Lunar and Planetary Science Conference, L*, Abstract #1252.

Zolotov, M. Y. (2017). Aqueous origins of bright salt deposits on Ceres. *Icarus, 296*, 289-304. doi:10.1016/j.icarus.2017.06.018

Zolotov, M. Y. (2020). The composition and structure of Ceres' interior. *Icarus, 335*, 113404. doi:https://doi.org/10.1016/j.icarus.2019.113404

Geophysical Research Letters

Supporting Information for

Replenishment of near-surface water ice by impacts into Ceres' volatile-rich crust: Observations by Dawn's Gamma Ray and Neutron Detector

T. H. Prettyman[1], N. Yamashita[1], M. E. Landis[2], J. C. Castillo-Rogez[3], N. Schörghofer[1], C. M. Pieters[1,4], Sizemore[1], H. Hiesinger[5], S. Marchi[6], H. Y. McSween[7], R. S. Park[3], M. J. Toplis[8], C. A. Raymond[3], C. T. Russell[9]

[1]Planetary Science Institute, Tucson, AZ. [2]Laboratory for Atmospheric and Space Physics, University of Colorado, Boulder, CO. [3]Jet Propulsion Laboratory, California Institute of Technology, Pasadena, CA. [4]Brown University, Providence, RI. [5]Institut für Planetologie, Westfälische Wilhelms-Universität Münster, Münster, Germany. [6]Southwest Research Institute, Boulder, CO. [7]University of Tennessee, Knoxville, TN. [8]L'Institut de Recherche en Astrophysique et Planétologie (University of Toulouse, UT3, CNRS), Toulouse, France. [9]University of California Los Angeles, Los Angeles, CA.

Contents of this file

Text S1 to S4
Figures S1 to S3

Introduction

The supplementary information describes the collection, reduction, and mapping of high spatial resolution data acquired by the Gamma Ray and Neutron Detector (GRaND) in Dawn final mission phase (Text S1 and S2).

Text S3 describes a mineral mixing model used to estimate the concentration of hydrogen within and around Occator crater based on mineral maps derived from data acquired by Dawn's Visible and Infrared Mapping Spectrometer (VIR).

Text S4 provides an overview of the thermophysical ice stability model used to support the interpretation of the data.

Figure S1 demonstrates that the high-resolution GRaND data are sensitive to the presence of hydrogen within the interior of Occator crater and the ejecta blanket.

Figure S2 shows the longitudinal dependence of crater density and hydrogen concentration.

Figure S3 compares the pattern of large craters with the distribution of hydrogen.

Text S1. Data and corrections

The GRaND data used in this study are available from the Planetary Data System (PDS) in PDS4 format:

https://sbn.psi.edu/pds/resource/dawn/dawngrandPDS4.html

In Dawn's final mission phase, GRaND acquired data in a highly eccentric orbit with a south-to-north trajectory around Ceres. The orbit was in a 3:1 resonance with Ceres (27h orbital period), which enabled acquisition of data along a selected meridian. The periapsides drifted along a great circle, starting in the western hemisphere north of Occator crater, gradually moving southward along the 240E meridian and crossing into the eastern hemisphere. The last data were acquired north of the equator in the eastern hemisphere along the antimeridian (60E) (Fig. 1a).

Data acquired between 8-Jun and 26-Oct of 2018, just prior to end-of-mission (1-Nov) were used. During this time, the spacecraft completed 123 eccentric orbits, with periapsides ranging from less than 30 km near the equator to about 55 km near the South Pole (Fig. 1b). Data from 10 orbits for which the main antenna was Earth-pointed were discarded. The remaining 113 orbits were used in the analysis, which included 60690 science data records. Of these, 540 records (0.9%) were flagged as invalid and removed, leaving 60,145 data records for use in the analysis. To ensure ample spatial sampling of the surface, the accumulation time for science data records was commanded to 35s for altitudes below about 1200 km. At higher altitudes, the accumulation time was set to 455s.

The data were acquired under quiet Sun conditions. No data were discarded due to solar activity. Following previous work (Prettyman et al., 2012; Prettyman et al., 2017), the GRaND triples and higher order coincidence counter (triples+) was used as a proxy for the flux of galactic cosmic rays, which interact with the regolith to produce gamma-rays and neutrons. At altitudes greater than a few body radii, contributions from secondary particles produced by cosmic rays are negligible. The altitude of apoapsis was about 4000 km (8.5 body radii), which enabled variations in the flux of galactic cosmic rays to be monitored every orbit. The triples+ rate measured at altitudes >6 body radii was resampled via linear interpolation to determine the variations in the cosmic ray flux for the entire time series.

At low altitudes (within a few body radii), thermal and epithermal neutrons originating from Ceres' surface interact with GRaND's +Z lithium-loaded glass scintillator via the $^{6}Li(n,\alpha)$ reaction. This reaction makes a peak in the CAT1 pulse height spectrum, which can be analyzed to determine the reaction rate (Prettyman et al., 2011). The peak area was determined for each science accumulation interval by subtracting a background spectrum measured at high altitude from a region-of-interest containing the peak (see Fig. 1c and Prettyman et al., 2017, supplement). For each measurement, the background spectrum was normalized to the continuum determined for each measurement from counts in a high energy region above the peak. The shape of the background was assumed to be the same for all measurements and was determined from high altitude measurements. The same approach for peak extraction was used in all previous studies (Prettyman et al., 2011; 2012; 2017).

The peak areas were divided by live time and corrections were applied to remove variations in the flux of galactic cosmic rays and measurement geometry. This produced a time-series of corrected interaction rates sensitive only to variations in surface composition. For measurement geometry, the $^{6}Li(n,\alpha)$ interaction rates were calculated at the mid-point location of each accumulation interval assuming the composition of Ceres' was homogeneous with a CI chondrite composition. The leakage current of neutrons (energy-angle distribution) for an arbitrary surface parcel was calculated using the Monte Carlo N-Particle eXtended transport code (McKinney et al., 2006). The Monte Carlo algorithm by Prettyman et al. (Prettyman et al., 2017; 2019) was used to model the response of the instrument to leakage neutrons at each orbital location, accounting for Ceres' shape and topography using a polygonal shape model determined from Framing Camera images using stereophotoclinometry (Park & Buccino, 2018; Park et al., 2019). The shape model was decimated to minimize compute times at high altitudes, where the instrument resolution is broader than the scale of surface features. For altitudes lower than 200 km, the mesh was decimated from 5123 to 2563 quadrilaterals, such that the mean distance between mesh points was about 3 km. This is sufficient to model the geometry of large-scale features such as Occator crater. Normalizing the measurements to simulated counts for a homogeneous surface removes artifacts of Ceres' shape and topography.

Text S2. Hydrogen mapping

The corrected $^{6}Li(n,\alpha)$ interaction rates were mapped onto the surface of Ceres using a circle superposition algorithm that accounts for variations in the spatial resolution of the instrument with altitude. Individual measurements are sensitive to the composition within an approximately circular surface region centered at the subsatellite point. The diameter of the circle is given by the spatial resolution of the spectrometer, which varies in proportion to altitude (e.g., Prettyman et al., 2019). For each measurement, the corrected interaction rate is uniformly distributed on the surface within the corresponding circle. The surface contributions from all the measurements are then averaged together to form a map.

Circle superposition approximates the double convolution of surface features by the response function of the spectrometer, which is a conservative approach for detection of variations in surface composition. The method is a robust extension of mapping algorithms that place measurements at the subsatellite point (Maurice et al., 2004). Circle superposition accounts for the widely varying spatial influence and limited spatial sampling of the measurements acquired in the eccentric orbits.

The maps presented in Figs. 2 and 3 were constructed from 5088 measurements acquired below 100 km altitude with the instrument pointed to within 20 degrees of body center. For the selected measurements, the average pointing angle was 4.8 degrees, with a population standard deviation of 3.5 degrees. Most of the data (98%) was acquired with a pointing angle <12 degrees, with 94% within 10 degrees and 59% within 5 degrees. This is consistent with the quality of the pointing data used for hydrogen mapping in LAMO, for which the cutoff was 12 degrees (Prettyman et al., 2017).

Selection of measurements made below 100 km provided ample spatial coverage to examine global latitude variations observed previously in LAMO (Prettyman et al., 2017), with at least 3× higher spatial resolution. We used 1.5 as the factor relating altitude to spatial resolution, consistent with previous studies of low-altitude data sets (Haines et al., 1978; Lawrence et al., 2003; Prettyman et al., 2009), and conservatively larger than predicted for the lithium-loaded glass scintillator at LAMO altitudes (Prettyman et al., 2019). Map values within the point cloud are insensitive to moderate variations in the scaling factor. Mapped variations in regions outside the point cloud are an extrapolation of the data and may not be as accurate as points inside the cloud. Regions with high confidence are bounded by white contours in Figs. 2 and 3. Points within this region have been sampled at least 50 times. The maximum spatial resolution (minimum full width at half maximum arc length on the surface) supported by the data is about 50 km, given the minimum altitude sampled was about 30 km. This scale is indicated by the circle in Fig. 2c.

The distribution of hydrogen was determined from the mapped corrected interaction rates using the method described by Prettyman et al. (2017). For comparison, the counting data within 20 degrees of the equator were normalized to match the values acquired previously in LAMO. This accounted for differences in counting rates resulting from changes in instrument settings, drifts in gain, and changing solar conditions between LAMO and high-resolution observations made near the end of the mission. Hydrogen concentrations derived from thermal and epithermal counting data are subject to systematic contributions from other elements. Based on modeling of Ceres analog materials, this source of uncertainty is smaller than 1 wt.% eq. H_2O (Prettyman et al., 2017).

The statistical uncertainty (1-sigma) in mapped hydrogen concentrations was determined using Monte Carlo error propagation, given estimates of the uncertainty in the measurements. The circle superposition algorithm was applied to 100 random samples of the time-series counting data. The population standard deviation is indicated by the vertical lines in Fig. 2b.

Text S3. Mineral mixing model

Maps of mineral mixing fractions in the Occator region were determined from VIR spectra by (Raponi et al., 2019) by least squares fitting of spectral end-members. These included Mg-, Al-, and NH_4-bearing phyllosilicates, Mg- and Na-carbonates, ammonium chloride, and a dark component. Following previous studies (Marchi et al., 2019; McSween et al., 2017; Prettyman et al., 2017; 2019), the reported mixing fractions were interpreted as volume fractions, which were used to determine hydrogen concentrations given approximate mineral structural formulae and densities. A map of hydrogen concentrations derived from VIR mineralogy is shown in Fig. 3a.

Note that the dark component is spectrally featureless in the near infrared, consistent with a mixture of magnetite, troilite, and partially hydrated, amorphous carbon (De Sanctis et al., 2015); however, the spectral mixing fraction for this component is very high outside the faculae, greater than 0.9 in some locations. With such high mixing fractions, no combination of spectrally featureless minerals can match ice-free concentrations of hydrogen and iron determined by GRaND. Instead, we modeled the dark component as the global average composition inferred simultaneously from GRaND and VIR data (Table 1, Case B of Marchi et al. (2019), which includes featureless components as well as contributions from hydrated minerals and carbonates. This gives the correct hydrogen content for dark materials representative of the global regolith, while allowing variability in hydrogen contributions from specific minerals identified by (Raponi et al., 2019) within the Occator region. Our ad hoc approach for estimating hydrogen concentrations is justified given the large uncertainties involved in interpreting VIR-derived spectral mixing fractions as mineral abundances (McSween et al., 2017).

The VIR-derived hydrogen map (Fig. 3a) only includes lattice water and hydrogen in amorphous carbon. At depths greater than the optical surface, bound water (i.e., to salts and in the interlayer of clay minerals) may be present along with water ice. The mineral mixing model results in relatively low concentrations of hydrogen in the faculae (as low as 8 wt.% eq. H_2O) compared to their dark surroundings (about 17 wt.% eq. H_2O).

Text S4. Thermophysical model

Thermophysical models for water ice stability were run based on a temperature model (Landis et al., 2017; Landis et al., 2019) utilizing orbital parameters determined by the Dawn mission. Our model matches other numerical calculations for Ceres surface and subsurface temperatures (Prettyman et al., 2017; Schorghofer, 2016). The modeled temperatures were used in a Knudsen-diffusion model previously developed for airless bodies (Schorghofer, 2008). The diffusive loss of water vapor determines the thickness of regolith that builds up, and further buries the ice-bearing layer. The following parameters and assumptions were used:

- Grain sizes from the analysis of VIR data for lobate deposits on the floor of Occator crater and the ejecta blanket (~110- and 70-μm, respectively) (Raponi et al., 2019) were used to estimate the vapor diffusion coefficient (see Fig. 3b).
- Thermal inertia of 15 SI units for the over-lying lithic sublimation lag (Rivkin et al., 2011) is used for the thermal model.
- Regolith surface single-scattering albedo of 0.09 (Carrozzo et al., 2018; Li et al., 2016).
- Obliquity, argument of perihelion from Dawn mission results (Russell et al., 2016).
- Depth-to-ice values are not significantly affected by the ~25 kyr obliquity cycles over the lifetime of Occator (Landis et al., 2017; Schorghofer, 2016).
- Shadowing from crater walls is negligible due to Occator's relatively large diameter and relatively flat floor.
- The initial sublimation lag depth is 3 cm, which represents a barrier to diffusion. This lag depth is also many times the diurnal skin depth in Ceres' desiccated regolith. We assume the temperature of the ice is equal to the annual average surface temperature.

To estimate water loss from hydrated salts, we modified the model by assuming (1) the buried water-bearing salt was natron ($Na_2CO_3 \cdot 10H_2O$), (2) the temperature of the natron was equal to the annual average surface temperature calculated for the regolith given the aforementioned parameters, and (3) all water molecules released from natron are lost instantaneously (the molecules did not condense to form ice or rehydrate the natron). We calculated the salt dehydration rate using the Arrhenius equation with constants derived from experiments of natron dehydration under Europa-like conditions (McCord et al., 2001). We found that at Occator crater, natron within the subsurface dehydrated on short timescales compared to the crater's estimated age of 20 Myr (Scully et al., 2019). This is consistent with the detection of only dehydrated sodium carbonate at Occator (Raponi et al., 2019). This supports the conclusion that hydrated sodium carbonate is unlikely to be a major contributor of water in the shallow sub-surface compared to water ice.

Recent work (Bu et al., 2018a; Bu et al., 2018b) has suggested that the dehydration of salts on Ceres depends also on grain size. It suggests that the grain sizes used in McCord et al. (2001), were large enough to add additional dehydration time due to the diffusion of water vapor through the grain itself. Therefore, dehydration times based on constants for the Arrhenius model from McCord et al. (2001), are possibly only upper limits.

Other hydrated salts such as hydrohalite ($NaCl{\cdot}2H_2O$), which was detected by VIR in Ceralia Facula (De Sanctis et al., 2020), and nahcolite ($NaHCO_3$), which degrades to form $NaCO_3$ under conditions present on Ceres' surface (Zolotov, 2017), are not likely a significant source of H. For example, even if nahcolite were concentrated in the shallow subsurface, it could account for no more than 11 wt.% equivalent H_2O. Experiments and modeling indicate the dehydration times for these minerals are also short compared to geologic time (Bu et al., 2018a; Bu et al., 2018b; Zolotov, 2017). Without the high pressures needed to re-hydrate these minerals, it is unlikely that they contribute as much hydrogen as water ice in the Occator region.

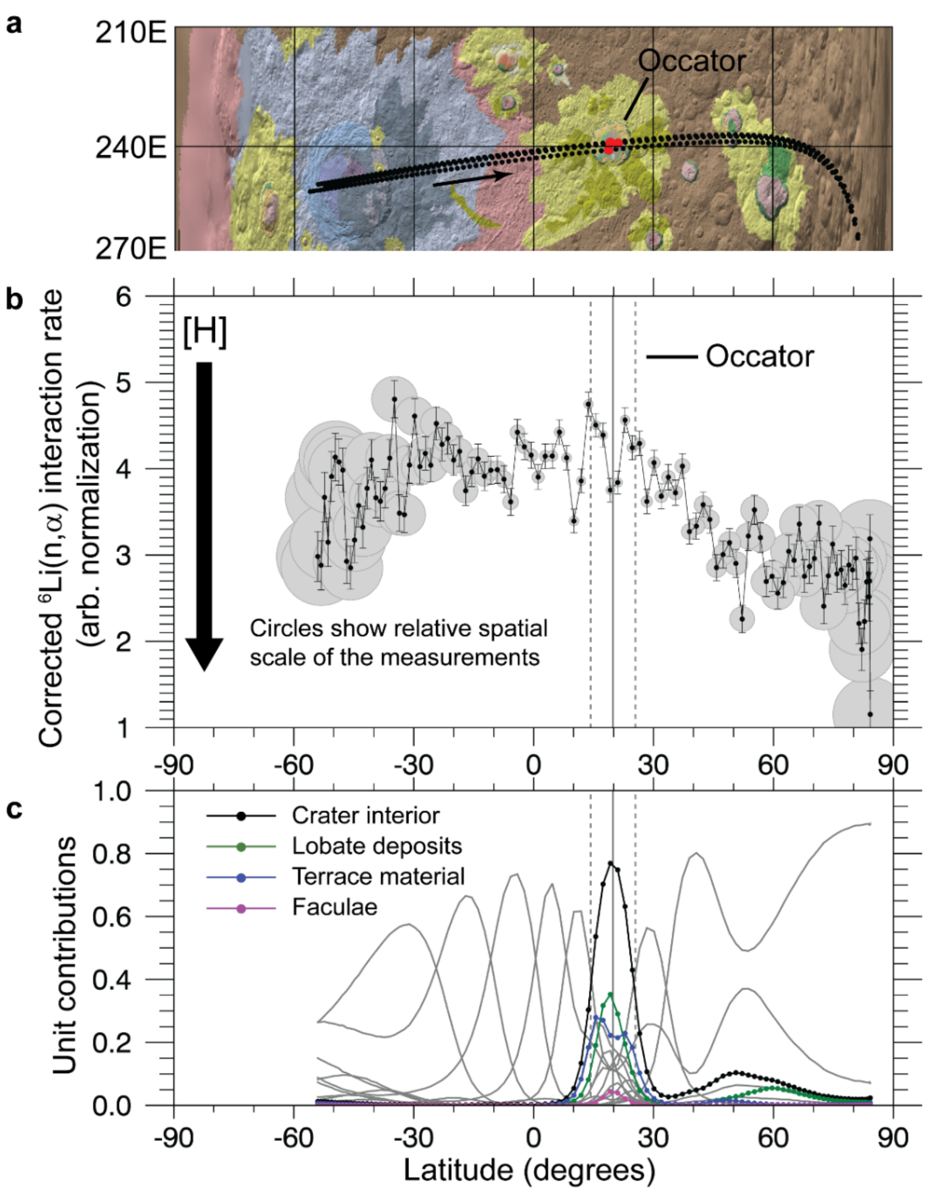

Figure S1. Spatial sensitivity of GRaND to geologic units within Occator crater. (a) Three orbits with nearly identical trajectories passing through the center of Occator crater are superimposed on a geologic map of Ceres (Williams et al., 2019). Locations of measurement center points (black circles) are plotted. The points of closest approach (about 35-km altitude) are highlighted in red. **(b)** The measured ^{6}Li(n,α) interaction rate averaged over the three orbits is shown (error bars indicate 1σ statistical precision). The dip within the crater boundary (dashed lines) is interpreted as elevated [H] within the crater interior. **(c)** A simulation of the response of GRaND to neutrons emitted from geologic units shows that the instrument is sensitive to the composition of the crater interior. The contribution from the faculae is negligible compared to lobate deposits and terrace material, which are possible locations for subsurface ice.

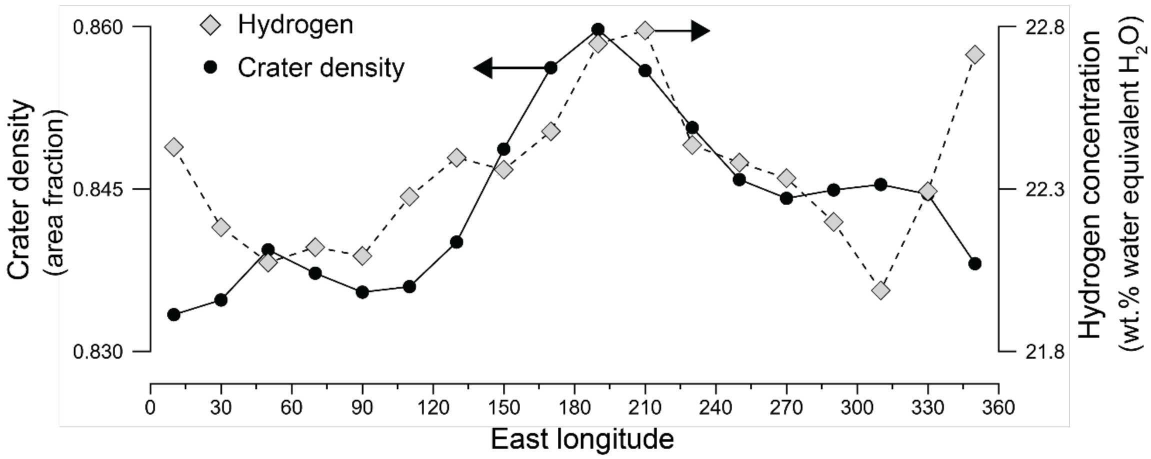

Figure S2. Longitudinal dependence of large craters and hydrogen concentration. The chart shows averages of the 20-degree equal area maps of crater density and hydrogen concentration (Fig. 4a) taken along meridians separated by 20 degrees longitude. The longitudinal variation in hydrogen concentration with crater density is correlated ($r = 0.55$). Given the coefficient of determination ($r^2 = 0.30$), the variation in hydrogen concentration is reduced by 30% when crater density is used as a predictor. As described in the main text, both crater density and hydrogen concentration have a broad maximum near 180E longitude.

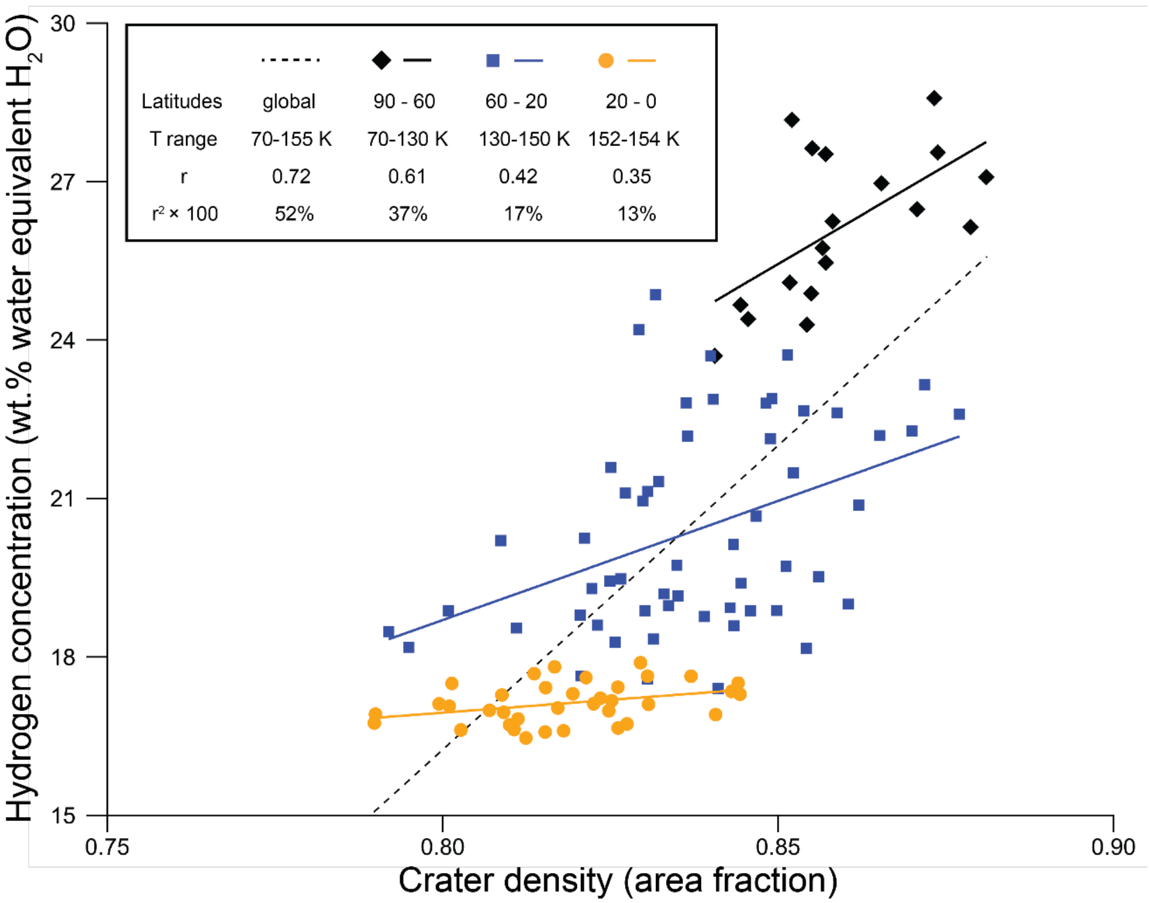

Figure S3. Comparison of the pattern of large craters and the distribution of hydrogen. Scatter plot of the density of large craters (20-100 km diameter) versus the concentration of hydrogen using data presented in Fig. 4a (see caption for the definition of crater density and data sources). The coefficient of determination (r^2) indicates strength of correlation and gives the fractional reduction in the variability of hydrogen that occurs when crater density is used as a predictor (see legend). The correlation is strong when all data points are considered; however, the concentration of hydrogen sensed by GRaND depends on the depth of subsurface water ice, which is controlled by near-surface temperature. Annual averaged surface temperatures, which vary with latitude with nearly hemispheric symmetry, were estimated using the model described in Text S4. The independent variable (crater density) is anticorrelated with temperature ($r = -0.64$). As a result, temperature is a confounding variable. To control for temperature, we divided the data set into three latitude ranges (combining N and S latitude bands). The distribution of large craters accounts for a portion of the variability within the selected ranges, which supports our replenishment hypothesis; however, the strength of correlation is such that processes other than impacts must also affect regolith hydrogen content.